The Astrophysical Journal, 750:41 (8pp), 2012 May 1 doi:10.1088/0004-637X/750/1/41

ON THE OCCURRENCE OF THE THIRD-ORDER SCALING IN HIGH LATITUDE SOLAR WIND

R. Marino[1,2], L. Sorriso-Valvo[3], R. D'Amicis[1], V. Carbone[3,4], R. Bruno[1], and P. Veltri[4]
[1] IFSI-INAF, via Fosso del Cavaliere, 00133 Roma, Italy; raffaele.marino@fis.unical.it
[2] Computational and Information Systems Laboratory, NCAR, P.O. Box 3000, Boulder, CO 80307-3000, USA
[3] IPCF-CNR, U.O. Cosenza, Ponte P. Bucci, cubo 31C, 87036 Rende (CS), Italy
[4] Dipartimento di Fisica, Università della Calabria, Ponte P. Bucci, cubo 31C, 87036 Rende (CS), Italy
Received 2011 November 29; accepted 2012 February 23; published 2012 April 13

ABSTRACT

The occurrence and nature of a nonlinear energy cascade within the intermediate scales of solar wind Alfvénic turbulence represents an important open issue. Using in situ measurements of fast, high latitude solar wind taken by the *Ulysses* spacecraft at solar minima, it is possible to show that a nonlinear energy cascade of imbalanced turbulence is only observed when the solar wind owns peculiar properties. These are the reduction of the local correlation between velocity and magnetic field (weak cross-helicity); the presence of large-scale velocity shears; and the steepening and extension down to low frequencies of the turbulent spectra. Our observations suggest the important role of both large-scale velocity and Alfvénicity of the field fluctuations for the validation of the Yaglom law in solar wind turbulence.

Key words: magnetohydrodynamics (MHD) – solar wind – turbulence

1. INTRODUCTION

The properties of solar wind turbulence have been deeply investigated in the last decades. Since the first power-law spectra of solar wind fields were obtained using spacecraft measurements, low frequency solar wind turbulence has been studied in the framework of nearly incompressible magnetohydrodynamics (MHD; Bruno & Carbone 2005). However, the actual nature of solar wind turbulence and the adequacy and range of validity of an MHD description are still open questions. In recent years, the linear scaling of the third-order moment of the field fluctuations (a Von Kármán–Howarth relation, also known as the *Yaglom law*; Monin & Yaglom 1975), observed in ecliptic (MacBride et al. 2005; Marino et al. 2011) and polar (Sorriso-Valvo et al. 2007) solar wind, has supported the MHD nature of the turbulent cascade. In this work, we describe the physical properties of polar, fast solar wind associated with the observation of the Yaglom law. This will provide new insights on the nature of the low frequency turbulent cascade in solar wind.

Incompressible MHD equations can be written in terms of the Elsässer variables $\mathbf{z}^{\pm} = \mathbf{v} \pm \mathbf{b}$ ($\mathbf{v}$ is the plasma velocity, $\mathbf{b} = \mathbf{B}/\sqrt{4\pi\rho}$ is the normalized magnetic field, and ρ is the plasma mass density), representing typical plasma fluctuations propagating along the large-scale magnetic field, as

$$\frac{\partial \mathbf{z}^{\pm}}{dt} \mp (\mathbf{B_0} \cdot \nabla)\, \mathbf{z}^{\pm} + \left(\mathbf{z}^{\mp} \cdot \nabla\right) \mathbf{z}^{\pm} = -\nabla P + D^{\pm} \,. \qquad (1)$$

Here, P is the total pressure (magnetic plus kinetic), $\mathbf{B_0}$ is the large-scale mean magnetic field, while $D^{\pm}$ indicate possible dispersive and dissipative mechanisms occurring in a collisionless plasma such as solar wind, replacing the usual viscous and resistive ∇^2 dissipative terms (Sorriso-Valvo et al. 2010). Nonlinear terms $(\mathbf{z}^{\mp} \cdot \nabla)\mathbf{z}^{\pm}$ in Equation (1) allow transfer of energy between fluctuations at different scales, originating the turbulent cascade responsible for the formation of the typical Kolmogorov frequency spectrum $\sim f^{-5/3}$ (Kolmogorov 1941) within intermediate scales. It should be pointed out that when velocity and magnetic fluctuations are highly correlated (maximal cross-helicity state), one of the two fields $\mathbf{z}^{\pm}$ has vanishing fluctuations. The mixed nonlinear terms $(\mathbf{z}^{\mp} \cdot \nabla)\mathbf{z}^{\pm}$ of MHD equations should then become negligible, consequently inhibiting the turbulent cascade and the formation of the spectrum (Dobrowolny et al. 1980; Bruno & Carbone 2005). In situ observations of fast solar wind plasma and the magnetic field show that the Kolmogorov-type spectrum for turbulent fluctuations within the inertial range (say from hours to a few seconds; Bruno & Carbone 2005), is commonly associated with a large correlation between velocity and magnetic field fluctuations (Belcher & Davis 1971; imbalanced Alfvénic MHD turbulence). MHD models for Alfvénic solar wind turbulence assume the existence of an energy cascade and aim at describing its development in an anisotropic turbulent medium. The Iroshnikov–Kraichnan phenomenology (Iroshnikov 1963; Kraichnan 1965) predicts the weakening of nonlinear interactions by the sweeping due to the large-scale Alfvénic fluctuations. This leads to the energy spectrum $f^{-3/2}$, also for a small-scale maximal cross-helicity state (Dobrowolny et al. 1980). A model for anisotropic strong MHD turbulence with zero cross-helicity has also been proposed (Goldreich & Sridhar 1995), based on the critical balance between the linear propagation and nonlinear interaction timescales. More recently, other phenomenological models have been developed (Grappin et al. 1983; Lithwick et al. 2007; Beresnyak & Lazarian 2008; Chandran 2008; Perez & Boldyrev 2009; Podesta & Bhattacharjee 2010; Gogoberidze et al. 2009). The vast literature on the subject (see Bruno & Carbone 2005 and reference therein) provided relevant advances, resulting from the observed spectra and related phenomena, such as intermittency (Sorriso-Valvo et al. 1999). Nevertheless, the proof of an MHD turbulent cascade for imbalanced solar wind turbulence has only been provided in recent years (MacBride et al. 2005; Sorriso-Valvo et al. 2007). This was achieved through the validation of the Von Kármán–Howarth scaling relation, also known as the Yaglom law for MHD, or Politano–Pouquet law. Turbulent field increments at a given position $\mathbf{x}$ and separation ℓ are usually described through the differences $\Delta\mathbf{z}^{\pm}(\ell; \mathbf{x}) = \mathbf{z}^{\pm}(\mathbf{x} + \ell) - \mathbf{z}^{\pm}(\mathbf{x})$. Under the hypotheses of stationarity, incompressibility, local isotropy and homogeneity, and within the inertial range, the Von Kármán–Howarth scaling law for the mixed third-order moments of the longitudinal field increments reads (Politano &

Pouquet 1998; Carbone et al. 2009b)

$$Y^{\pm}(\ell) = \left\langle |\Delta \mathbf{z}^{\pm}(\ell; \mathbf{x})|^2 \, \Delta z_R^{\mp}(\ell; \mathbf{x}) \right\rangle = -\frac{4}{3} \epsilon^{\pm} \ell \, , \qquad (2)$$

where $z_R^{\mp}$ indicate the longitudinal component (i.e., radial in the usual RTN coordinate system) of the Elsässer fields, and $\ell \parallel R$. Angle brackets indicate space average, computed over the whole field. The turbulent cascade pseudo-energy fluxes $\epsilon^{\pm}$, customarily defined as the trace of the dissipation rate tensors $\epsilon_{ij}^{\pm} = \nu \langle (\partial_i z_i^{\pm})(\partial_i z_j^{\pm}) \rangle$), describe the energy transfer rates between Elsässer field structures on scales within the inertial range of MHD turbulence. Note that the Yaglom law is valid only if the pseudo-energy transfer rates $\epsilon^{\pm}$ remain finite in the limit of vanishing viscosity and resistivity. This hypothesis has not been tested in the solar wind so far. The application of the Taylor hypothesis, well verified in fast solar wind, is necessary to switch from spatial scales ℓ to timescales τ, using $\ell = -\langle v_R \rangle \tau$ (brackets indicating here time averages over the whole time series). Equation (2) was first observed in the inertial range of two-dimensional MHD numerical simulations (Sorriso-Valvo et al. 2002). The successive observation in solar wind samples (MacBride et al. 2005; Sorriso-Valvo et al. 2007) proved that intermediate-scale solar wind fluctuations can be described within the MHD model of turbulence. However, it was reported that the scaling is not present everywhere in the data sets, but rather sets up under particular conditions (Sorriso-Valvo et al. 2007), which constitute the focus topic of this paper. The fit of experimental data with Equation (2) gives an estimate of the pseudo-energy transfer rates $\epsilon^{\pm}$, which can be used as a proxy for the total energy transfer rate (Marino et al. 2008; Sorriso-Valvo et al. 2010). Observed values are strongly variable, in the range 0.05–10 kJ kg^{-1} s^{-1}. The values in polar wind are an order of magnitude smaller than in the ecliptic (Sorriso-Valvo et al. 2007; Marino et al. 2008, 2011; Smith et al. 2009). The phenomenological inclusion of density fluctuations in the Yaglom law provides a relevant enhancement of the energy transfer rate. This has been observed in solar wind data (Carbone et al. 2009a), and recently discussed theoretically (Galtier & Banerjee 2011). In the ecliptic wind, energy transfer rates anti-correlate quite well with the Alfvénicity (Smith et al. 2009), evaluated as customary through the normalized cross-helicity (Goldstein et al. 1986):

$$\sigma_c = 2\langle \Delta \mathbf{v} \cdot \Delta \mathbf{b} \rangle / (\langle \Delta \mathbf{v}^2 \rangle + \langle \Delta \mathbf{b}^2 \rangle). \qquad (3)$$

It should be stressed that the energy transfer rate estimated through Equation (2) only represents the purely incompressible, homogeneous, isotropic, MHD contribution to the cascade, because it disregards possible terms that could modify the results (Politano & Pouquet 1998; Carbone et al. 2009b). Within this approximation, ecliptic observations are thus in agreement with the inhibition or reduction of the nonlinear cascade for highly Alfvénic turbulence. However, the reasons for the irregular observation of the cascade in samples of polar, high Alfvénic wind are still unclear.

2. ANALYSIS OF *ULYSSES* DATA

The present analysis was performed using *Ulysses* eight minute resolution measurements of velocity, magnetic field, and plasma density (Smith et al. 1995b; Balogh et al. 1995), sampled in about 2×10^5 running windows 11 days long (Sorriso-Valvo et al. 2007; Marino et al. 2008, 2011). The window size was selected to be large enough as to include several correlation lengths (typically of the order of a few hours up to a few days, in order to ensure ergodicity, but short enough as to provide reasonable stationarity of the sample within each window (Sorriso-Valvo et al. 2007)). Furthermore, to reduce as much as possible the presence of disturbances of solar origin, only fast wind measurements taken far from the ecliptic, during low solar activity, have been used. Figure 1 shows the radial velocity profile, together with the orbital parameters of *Ulysses*. Three time intervals, each $\sim$ one year long, have been selected (from DoY 209/1993 to 253/1994; from 212/1995 to 224/1996; and from 20/2006 to 23/2007, see Figure 1), so that each data set (corresponding to a semi-orbit of the *Ulysses* spacecraft) has comparable variation of radial distance ($\sim$2–4.5 AU) and heliolatitude ($\sim$30°–80°, north or south). Semi-orbit I was taken during the solar activity decrease, near a minimum; semi-orbit II at solar minimum; semi-orbit III was taken during the decrease, very close to the recent anomalous minimum (Wang et al. 2009). The Yaglom law (Equation (2)) has been systematically evaluated in the whole data set. Figure 2 shows one example of linear scaling as observed in one particular 11 day window. The scaling is observed in a relevant fraction of windows, where local conditions enable a homogeneous, isotropic, incompressible MHD cascade contribution to turbulence (Sorriso-Valvo et al. 2007). Note that the local isotropy hypothesis is a strong assumption for solar wind turbulence. The anisotropic version of the Von Kármán–Howarth scaling law has been derived for plasmas (Galtier 2011), and simplified models based on assumptions on the solar wind turbulence anisotropy have been used (Stawarz et al. 2011). However, a full anisotropic description would require the estimation of three-dimensional gradients, which are not at reach with the available measurements. Therefore, in this paper we use the isotropic scaling law, assuming that the observation of the scaling corresponds to samples where anisotropy effects are negligible. For the particular case illustrated in Figure 2, the linear range extends from 1 hr to about 48 hr (Goldstein et al. 1995). The smaller scale is bounded by the data resolution, which is one order of magnitude larger than the typical lower limit of the MHD inertial range (Leamon et al. 1998; Alexandrova et al. 2007, 2008). The large scale variates in the whole data set, from a few hours to a few (two to three) days. Such values are considerably larger than the commonly adopted correlation lengths (namely a few hours; Bruno & Carbone 2005), indicating that the local properties of the cascade can be strongly variable. We remind here that the mixed third-order scaling gives a more rigorous localization of the actual inertial range, with respect to the energy spectrum (see, e.g., Frisch 1995). It has been argued that large scales, such as the ones observed in our *Ulysses* data analysis, could lack causal connection (Zhou & Matthaeus 1990; Forman et al. 2010). However, a turbulent cascade on such scales is compatible with the possibility of an energy transfer locally induced by large-scale structures of solar origin (such as shears; Sorriso-Valvo et al. 2010). It should be pointed out that the use of windows considerably smaller or larger than 11 days leads to the loss of linear scaling, suggesting the local (rather than universal) character of solar wind MHD turbulence (Sorriso-Valvo et al. 2010).

After computing the mixed third-order moment for all running windows, a statistical analysis of the results was performed. The bottom panels of Figure 3 show the fraction of 11 day intervals where the Yaglom law was observed (namely, a linear scaling was found over at least one decade), indicated in this paper as "scaling ratio," and estimated within four statistically

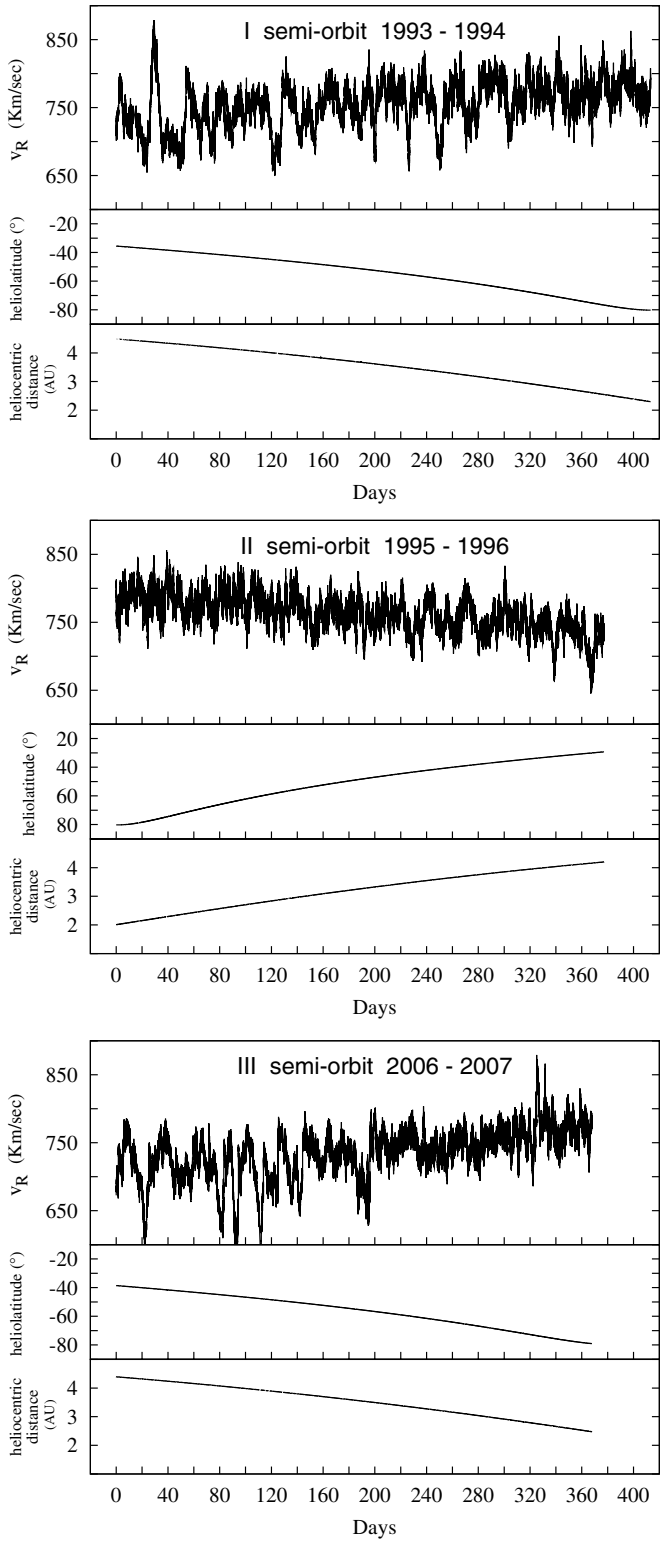

Figure 1. Radial velocity measurements taken by the *Ulysses* spacecraft, for the three time intervals used in the present paper. For each of the three figures, top panel: the radial velocity v_r, in km s^{-1}; center: the heliolatitude θ, in °; bottom: the heliocentric distance R, in AU.

homogeneous intervals at different heliolatitude and radial distance. The scaling ratio is smaller at high latitudes and closer to the Sun (about 10%), and increases considerably toward the poles and far from the Sun (approximately 30%). This indicates that turbulence, or at least the conditions for the observation of

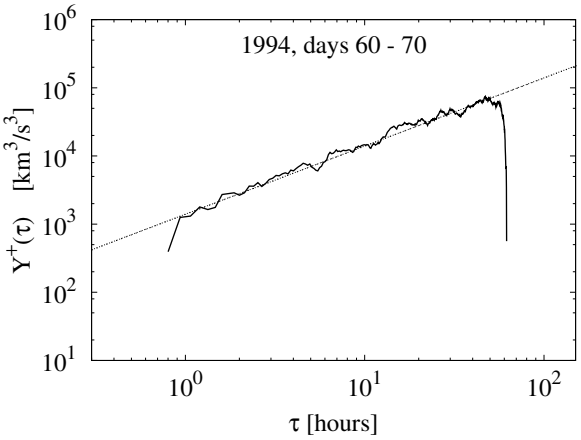

Figure 2. Example of linear scaling of the mixed third-order moment Y^+ for one particular sample of data (from day 60–70 of the year 1994). The linear fit is also plotted (dotted line).

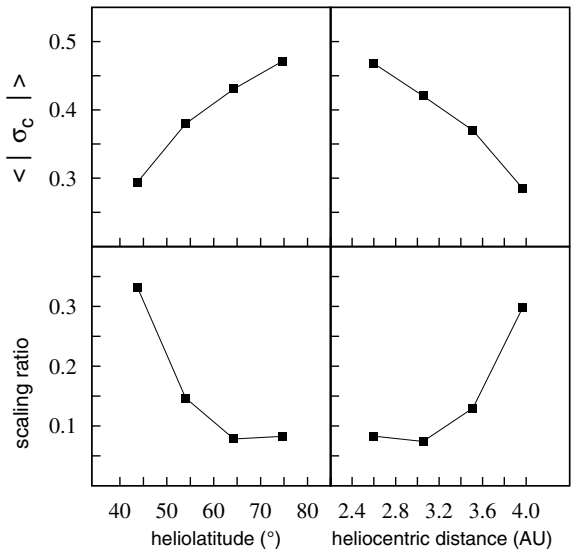

Figure 3. Latitudinal and radial variation of the mean cross-helicity (top) and scaling ratio (bottom). Values have been computed by evaluating the normalized cross-helicity $|\sigma_c|$ and the scaling ratio for each of the 11 day windows, and then averaging over four bins of heliolatitude and radial distance.

the Yaglom law, changes significantly during the solar wind expansion in the heliosphere. The top panels of Figure 3 show the absolute value of normalized cross-helicity, computed inside each 11 day window, and then averaged over the same heliolatitude and radial distance bins as in the bottom panels. As expected, $\langle|\sigma_c|\rangle$ (brackets indicating here the average computed over the windows) increases at higher latitudes, confirming the enhancement of outgoing Alfvénic fluctuations in the fast wind coming from coronal holes (Smith et al. 1995a), and decreases with the radial distance, in agreement with previous observations of radial decay of Alfvénic fluctuations (Bavassano et al. 2000). This was also predicted, for example, through a numerical study of the MHD parametric instability (Malara et al. 2000). We point out that, because of the *Ulysses* orbital parameters, it is not possible to discriminate whether the observed orbital dependence is due to the distance or to the heliolatitude. However, our data are taken far from the ecliptic, within fast wind, so that the latitudinal variation should not affect the wind properties (Bavassano et al. 2002). A quick look at Figure 3

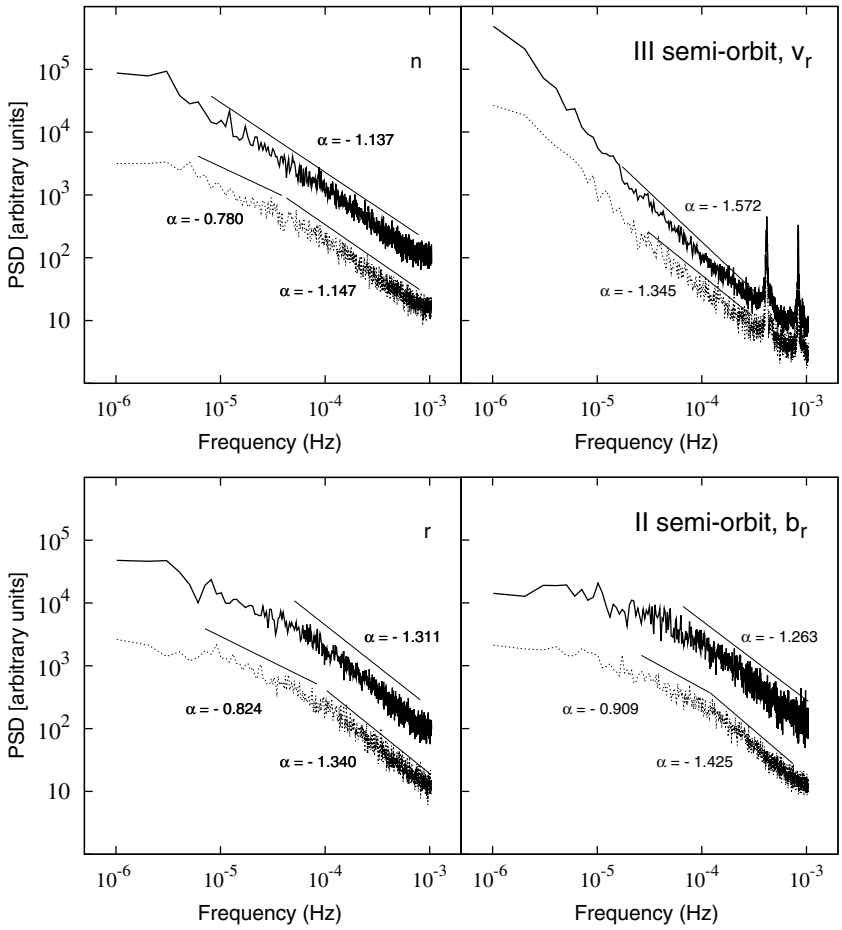

Figure 4. Examples of velocity (top panels) and magnetic field (bottom panels) components power spectra. The spectra are computed separately for regions with (full line) and without (dashed line) Yaglom scaling. Spectra have been vertically shifted for clarity and are given in arbitrary units. Solid lines are power-law fits of the spectra, also vertically shifted for clarity. The spectral indices obtained by the fit are given in the following. Top left panel, solid line: $\alpha = -1.137 \pm 0.001$; dashed lines: -0.780 ± 0.004 and -1.147 ± 0.002. Top right panel, solid line: $\alpha = -1.572 \pm 0.006$; dashed lines: $\alpha = -1.345 \pm 0.006$. Bottom right panel, solid line: $\alpha = -1.263 \pm 0.002$; dashed lines: $\alpha = -0.909 \pm 0.004$ and $\alpha = -1.425 \pm 0.003$. Bottom left panel, solid line: $\alpha = -1.311 \pm 0.002$; dashed lines: $\alpha = -0.824 \pm 0.002$ and $\alpha = -1.340 \pm 0.003$. The two peaks present at high frequency in the v_R spectra are due to the plasma instrument data acquisition logic, see http://ulysses-ops.esa.int/ulysses/.

shows an evident qualitative anti-correlation between the scaling ratio and $\langle|\sigma_c|\rangle$. Thus, the smaller the imbalance, the higher the probability of observing linear scaling of the mixed third-order moment. Values of scaling ratio and mean cross-helicity can also be computed separately for each semi-orbit, disregarding the orbital variation (Figure 6). The two parameters, which are again qualitatively well correlated, are considerably different for the three samples. In particular, both first and third semi-orbits have scaling ratio of about 50%, and quite small mean cross-helicity ($\langle|\sigma_c|\rangle \simeq 0.2$). On the contrary, the second semi-orbit shows a lack of linear MHD scaling regions (about 10% of the whole orbit), with a larger average value of the mean cross-helicity ($\langle|\sigma_c|\rangle \simeq 0.5$). This underlines the substantial differences between each orbit, evidencing the need for a separate analysis. Based on the above considerations, in order to investigate the irregular presence of the MHD cascade in Alfvénic solar wind turbulence, we now split the data into two classes, namely with (data set 1) and without (data set 2) linear scaling. Therefore, each of the two data sets has homogeneous physical properties, as long as the observation of the MHD cascade is concerned. We thus analyze averaged properties for each *Ulysses* polar semi-orbit, regardless of the radial distance and heliolatitude. This procedure should single out persistent properties of the solar wind turbulent fluctuations, related to the presence or absence of the MHD scaling. The two data sets have been thus studied separately, using diagnostic tools such as spectra and probability distribution functions (PDFs) of field fluctuations and of cross-helicity.

2.1. Spectral Properties of Solar Wind Fluctuations

In the phenomenological approach to turbulence, the properties of the energy spectra of the field fluctuations are often investigated. Although spectral analysis does not give a complete description of turbulence (e.g., it does not account for intermittency), it provides important information, as for example the identification of particular regimes, or the localization of characteristic scales (Frisch 1995). The normalized power spectra of the MHD fields $\mathbf{v}$, $\mathbf{b}$, $\mathbf{z}^{\pm}$ components have been computed separately for scaling and non-scaling 11 day windows, and then averaged over each of the three semi-orbits. Examples of spectra are shown in Figure 4. Spectral indices have been obtained through a standard power-law fit. All fields show power-law regions of variable extension, with exponents compatible with the typical Kolmogorov phenomenology (Frisch 1995), suggesting the presence of a nonlinear energy cascade. However, the observed spectral slope α is not universal (Horbury et al. 1995). The study of the averaged spectral properties leads to a loss of details on plasma conditions. On

the other hand, the selective average process highlights robust features that can give hints on the possible physical reasons for inhomogeneous observation of the Yaglom law. Note that, because of the data resolution, the small scales knee of the spectrum, indicating the bottom of the MHD inertial range and usually located at timescales of about several seconds, is not observed in the data (Leamon et al. 1998; Alexandrova et al. 2007, 2008). Furthermore, we point out that, from now on, we will use the terminology "Kolmogorov spectrum," or similar ones, to generically indicate values of the spectral index compatible with an inertial range turbulent cascade. In Figure 4, we show four examples of selectively averaged velocity and magnetic components spectra, in which the differences between scaling and non-scaling regions are more evident. In the samples without Yaglom scaling, the normal velocity component (v_N) spectra (top left panel) have on average a shallow spectrum in the low frequency range, while a steeper spectrum follows in the higher frequency range. In the data with scaling, the linear range extends to larger scales. More striking differences are observed for the radial component of the velocity (v_R), as shown in the top right panel. In this case, a sharp difference between the two sets is also present in the spectral index. In particular, Kolmogorov-type values of the slope $\alpha \simeq -1.5$ are observed, on average, for the Yaglom scaling regions, while shallower spectra with spectral slopes around $\alpha \simeq -1.2$ characterize the samples without Yaglom scaling. The magnetic field components also display differences between scaling and non-scaling regions. As suggested by the two examples shown in the second row of Figure 4, for the radial component the typical $1/f$ knee is shifted to larger scales (from about 3 to 6 hr) when the Yaglom law is observed. This is also the case, but less evident, for the other magnetic field components and for the Elsässer fields components (not shown).

To summarize the main differences, samples which satisfy Yaglom law are generally characterized by (1) a spectral index closer to the typical values for a turbulent phenomenology ($\alpha \simeq -1.5$); and (2) a turbulent power-law spectral range extending toward larger scales. It should be noted that the extension of the mixed third-order moment inertial range to large scales observed from *Ulysses* data (Sorriso-Valvo et al. 2007, 2010) is associated with a more extended linear range in the spectra. The observation of the Yaglom law in polar solar wind samples thus seems to be related to the presence of a Kolmogorov-type velocity spectrum on a wide range of scales, indicating a "classical" turbulent cascade. Conversely, regions where the Yaglom law is not observed have shallower slope, or a reduced extension of the linear range.

2.2. The Role of Large-scale Velocity Shears

The existence of power-law spectra indicates that scale free fluctuations are present at all scales within a given range. Spectral properties of velocity show differences between the scaling and non-scaling regions of the solar wind. More detailed information about the role of field fluctuations in the MHD turbulent cascade can be inferred through the PDFs of the field increments, e.g., $P([\Delta \mathbf{v}]_\tau)$, at different scales τ. PDFs are customarily used in turbulence studies to describe the scaling properties of the field fluctuations. They provide complete statistical characterization of the fluctuations, including, e.g., intermittency. In fact, intermittency can be evidenced through the tails enhancement of PDFs at smaller scales, indicating an increasing presence of localized (intermittent) energetic structures. Figure 5 shows the PDFs of velocity and magnetic field components and of the density, evaluated at three different scales, separately for scaling and non-scaling regions. The typical intermittent behavior, with rising tails at small scales, is present for all fields in our study. As already reported in the literature, magnetic field intermittency is stronger than other fields (Sorriso-Valvo et al. 1999). However, the separation between MHD Yaglom scaling and non-scaling regions yields to different behavior at large scales. With the exception of the magnetic field, PDFs of all fields are considerably wider in the case of Yaglom scaling, presenting fat tails. The latter are associated with the enhanced presence of large-scale shears. More particularly, the fatter positive tail of $P([\Delta v_R])$ observed at large scale (Figure 5) is a strong indication that radial velocity shears, characterized by a steep ramp followed by a slower speed decrease, are linked to the MHD turbulent cascade. Density fluctuation PDFs have symmetric tails, as expected for the typical density enhancements observed where velocity shears are present. Thus, the MHD Yaglom law is observed when large-scale velocity and density shears are present in the flow. Recent independent studies on ecliptic solar wind provided similar results (Stawarz et al. 2011). From our observation, it seems evident that the presence of large-scale velocity and density structures could represent the energy source for the turbulent cascade, as originally proposed by Coleman using Mariner 2 data (Coleman 1968), and later supported by numerical results (Roberts et al. 1992). In recent studies of ecliptic solar wind turbulence, the driving of the cascade by velocity shears has been ruled out by Borovsky & Denton (2010). However, only stream-interface shears were considered, which have different characteristics with respect to the shears studied here.

2.3. The Role of Cross-helicity and Solar Activity

The phenomenological arguments discussed above suggest that the degree of Alfvénic correlations is connected with the turbulent cascade (Dobrowolny et al. 1980). This was recently supported by observations in the ecliptic wind (Smith et al. 2009; Marino et al. 2011). In order to better highlight the role of cross-helicity for the observation of the cascade, we again separately analyze samples with or without the Yaglom scaling. Moreover, we also want to evaluate the possible influence of the different level of solar activity on the linear MHD Yaglom scaling. Indeed, the three semi-orbits analyzed here all refer to low solar activity periods, very close to minima. However, differences are still present in the activity level, which allow a comparative analysis.

The top panel of Figure 6 shows the mean solar activity, estimated through the green coronal emission line 530.3 nm observations, given in millionths of intensity of the solar disk (coronal units; Rybansky et al. 1994), integrated in the polar regions (40°–80° north or south) and then time averaged over the relevant periods. The figure also shows: the scaling ratio (second panel from the top); the mean normalized cross-helicity $\langle|\sigma_c|\rangle$ (central panel), evaluated by computing the absolute value of the normalized cross-helicity for each 11 day window, and then averaging over each semi-orbit, after separating regions with (solid line) and without (dashed line) the Yaglom scaling; the mean turbulent pseudo-energy transfer rate $\epsilon \simeq \epsilon^{\pm}$, estimated from the fit of the Yaglom law (Sorriso-Valvo et al. 2010; fourth panel from the top); and the mean value of rms($|\tilde{\sigma_c}|$) for each semi-orbit, where $\tilde{\sigma_c} = 2(\Delta \mathbf{v} \cdot \Delta \mathbf{b})/(\Delta \mathbf{v}^2 + \Delta \mathbf{b}^2)$ is the "local cross-helicity." The quantity $|\tilde{\sigma_c}|$ has been evaluated for every single point of the data set, so that the rms of ($|\tilde{\sigma_c}|$), computed over 11 day intervals, represents the degree of fluctuation of the

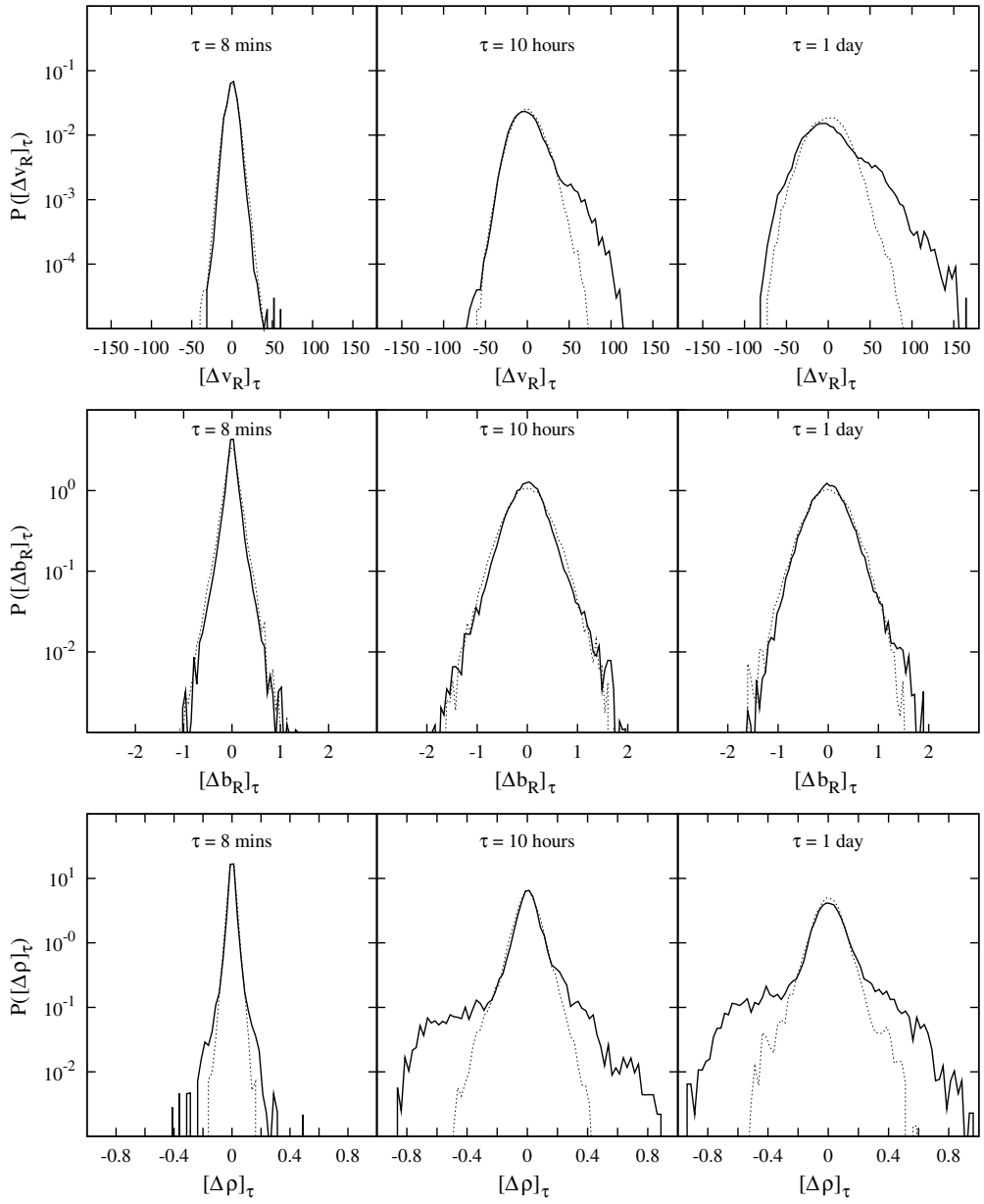

Figure 5. Probability distribution functions of field fluctuations for radial velocity (top), radial magnetic field (center), and density (bottom), at different time lags. For each plot, PDFs are computed separately for set 1 (Yaglom scaling: full line) and for set 2 (absence of Yaglom scaling, dotted line).

alignment between velocity and magnetic field in each 11 day window.

The values of $\langle|\sigma_c|\rangle$ and $\langle \mathrm{rms}(|\tilde{\sigma_c}|)\rangle$ are plotted separately for the regions with (squares, solid line) and without (circles, dashed line) scaling. Both the scaling ratio and the averaged pseudo-energy transfer rate correlate with the solar activity. In the II semi-orbit, characterized by very low solar activity, samples with scaling are rare (∼10%), while in the I and III semi-orbits, the enhanced solar activity produces a larger scaling ratio (∼50%). Moreover, anti-correlation between the absolute value of normalized cross-helicity and solar activity exists. Importantly, such anti-correlation only holds when the Yaglom scaling is present, while $\langle|\sigma_c|\rangle$ is roughly constant in the remaining samples, confirming the direct link between the presence of the MHD cascade and the cross-helicity. These observations suggest the importance of the solar input for solar wind MHD turbulence. The local variability of $|\sigma_c|$ could therefore explain the presence (and the irregular character) of the MHD cascade in the globally Alfvénic solar wind. Lower cross-helicity states are indeed associated with MHD scaling regions, while higher cross-helicity samples seldom satisfy the Yaglom law. The bottom panel of Figure 6 indicates a higher degree of fluctuations of the local alignment when the MHD cascade is observed. This further confirms that the correlation with solar activity and the energy transfer rate only exists for the MHD Yaglom scaling regions.

To resume, as the wind blows away from the Sun in the interplanetary space (see Figure 3), velocity and magnetic field fluctuations become less correlated, and the MHD Yaglom law is satisfied in a larger and larger fraction of data. This observation disagrees with the common MHD phenomenology of dynamical alignment (Boldyrev 2005), for which the system spontaneously evolves toward a large cross-helicity state (Dobrowolny et al. 1980). This suggests the possible need for an input mechanism

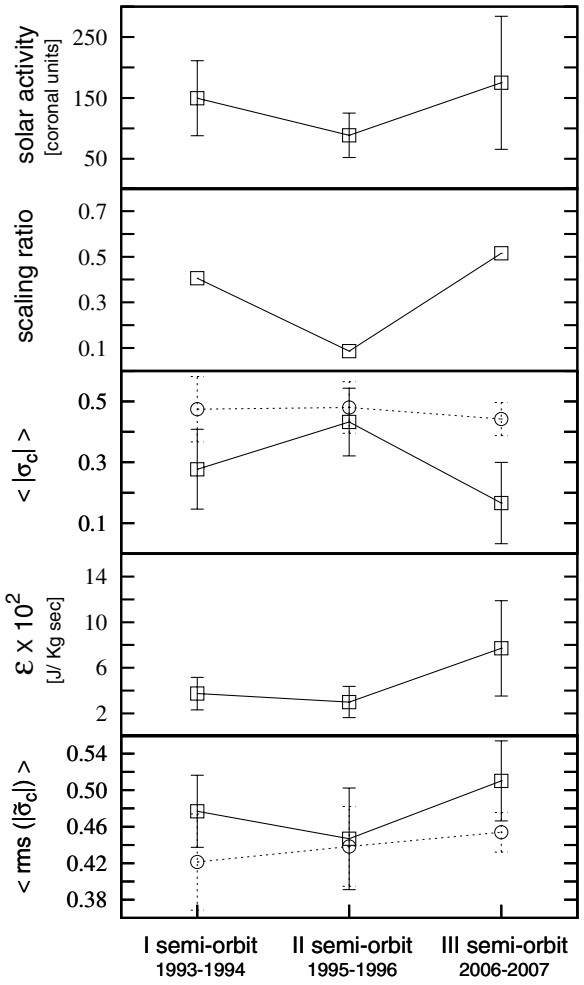

Figure 6. Average values of solar activity, scaling ratio, mean cross-helicity, pseudo-energy transfer rate, and rms local cross-helicity for the three semi-orbits. For the cross-helicity panels, full lines represent values for samples with MHD scaling, while dotted lines refer to regions without scaling.

for the decorrelation of the fields, and for the setup of the MHD turbulent cascade. This could be, for example, the velocity and density shears described in the previous section. Finally, the link between solar activity and observation of Yaglom scaling could be related to the enhanced energy input (e.g., in form of velocity and density shears) during higher solar activity.

3. DISCUSSION OF RESULTS

To conclude, we have selectively analyzed fast solar wind samples measured at high latitudes by the *Ulysses* spacecraft during solar minima, identifying two classes of wind, which have shown different features.

1. Regions without MHD Yaglom scaling have shallower spectra with a shorter kolmogorov-type range, the absence of large-scale velocity and density shears, also, they display larger $|\sigma_c|$ values and smaller fluctuations of the local cross-helicity. These are dominant in the II semi-orbit, and in most of the samples with $R < 3.5$ AU in the I and III semi-orbits (Figures 3 and 6).
2. Regions with fully developed MHD Yaglom scaling, mainly in the I and III semi-orbits at large distance from the Sun, are characterized by a spectral index close to typical turbulent values, and an extended kolmogorov-type range; they show large-scale velocity and density shears; and they are characterized by smaller $|\sigma_c|$ values and larger fluctuations of the local cross-helicity. These are seen mostly at larger distances from the Sun, where Alfvénic correlations decrease.

We have also pointed out the correlation between the MHD turbulent cascade (local and global cross-helicity, scaling ratio, and energy transfer rate) and the solar activity (including the enhanced presence of large-scale velocity and density shears), suggesting the direct importance of the solar input for the onset of the cascade. Finally, results shown here further confirm the non-universal nature of solar wind turbulence, and underline the importance of selecting homogeneous samples when performing statistical analysis of data. In particular, the Yaglom law has been proven to be a valid criterion to discriminate between different physical conditions.

This work was partially financed by ASI contract No. I/015/07/0 "Esplorazione del Sistema Solare"; L.S.V., R.M., R.B., and V.C. are part of ISSI team 185 "Dispersive cascade..."; L.S.V., V.C., and P.V. acknowledge FP7 PIRSES-2010-269297—"Turboplasmas"; R.M. acknowledges D. Gomez for helpful discussion.

REFERENCES

Alexandrova, O., Carbone, V., Veltri, P., & Sorriso-Valvo, L. 2007, Planet. Space Sci., 55, 2224
Alexandrova, O., Carbone, V., Veltri, P., & Sorriso-Valvo, L. 2008, ApJ, 674, 1153
Balogh, A., Smith, E. J., Tsurutani, B. T., et al. 1995, Science, 268, 1007
Bavassano, B., Pietropaolo, E., & Bruno, R. 2000, J. Geophys. Res., 105, 12697
Bavassano, B., Pietropaolo, E., & Bruno, R. 2002, J. Geophys. Res., 107, 1248
Belcher, J. W., & Davis, L., Jr. 1971, J. Geophys. Res., 76, 3534
Beresnyak, A., & Lazarian, A. 2008, ApJ, 682, 1070
Boldyrev, S. 2005, ApJ, 626, L37
Borovsky, J. E., & Denton, M. H. 2010, J. Geophys. Res., 115, A10101
Bruno, R., & Carbone, V. 2005, Living Rev. Sol. Phys., 2, 4
Carbone, V., Marino, R., Sorriso-Valvo, L., Noullez, A., & Bruno, R. 2009a, Phys. Rev. Lett., 103, 061102
Carbone, V., Sorriso-Valvo, L., & Marino, R. 2009b, EPL (Europhys. Lett.), 88, 25001
Chandran, B. D. 2008, ApJ, 685, 646
Coleman, P. J. 1968, ApJ, 153, 371
Dobrowolny, M., Mangeney, A., & Veltri, P. 1980, Phys. Rev. Lett., 45, 144
Forman, M. A., Smith, C. W., & Vasquez, B. J. 2010, Phys. Rev. Lett., 104, 189001
Frisch, U. 1995, Turbulence. The Legacy of A. N. Kolmogorov (Cambridge: Cambridge Univ. Press)
Galtier, S. 2011, C. R. Phys., 12, 151
Galtier, S., & Banerjee, S. 2011, Phys. Rev. Lett., 107, 134501
Gogoberidze, G., Mahajan, S. M., & Poedts, S. 2009, Phys. Plasmas, 16, 072304
Goldreich, P., & Sridhar, S. 1995, ApJ, 438, 763
Goldstein, B. E., Smith, E. J., Balogh, A., et al. 1995, Geophys. Res. Lett., 22, 3393
Goldstein, M. L., Roberts, D. A., & Matthaeus, W. H. 1986, J. Geophys. Res., 91, 13357
Grappin, R., Leorat, J., & Pouquet, A. 1983, A&A, 126, 51
Horbury, T. S., Balogh, A., Forsyth, R. J., & Smith, E. J. 1995, Geophys. Res. Lett., 22, 3401
Iroshnikov, P. S. 1963, SvA, 40, 742
Kolmogorov, A. N. 1941, Dokl. Akad. Nauk. SSSR, 30, 301
Kraichnan, R. H. 1965, Phys. Fluids, 8, 1385
Leamon, R. J., Smith, C. W., Ness, N. F., et al. 1998, J. Geophys. Res., 103, 4775
Lithwick, Y., Goldreich, P., & Sridhar, S. 2007, ApJ, 655, 269
MacBride, B. T., Forman, M. A., & Smith, C. W. 2005, in Solar Wind 11/SOHO 16, Connecting Sun and Heliosphere, ed. B. Fleck, T. H. Zurbuchen, & H. Lacoste (ESA-SP 592; Noordwijk: ESA), 613
Malara, F., Primavera, L., & Veltri, P. 2000, Phys. Plasmas, 7, 2866

Marino, R., Sorriso-Valvo, L., Carbone, V., et al. 2008, ApJ, 677, L71
Marino, R., Sorriso-Valvo, L., Carbone, V., et al. 2011, Planet. Space Sci., 59, 592
Monin, A. S., & Yaglom, A. M. 1975, Statistical Fluid Mechanics, Vol. 2 (Cambridge: MIT Press)
Perez, J. C., & Boldyrev, S. 2009, Phys. Rev. Lett., 102, 025003
Podesta, J., & Bhattacharjee, A. 2010, ApJ, 718, 1151
Politano, H., & Pouquet, A. 1998, Geophys. Res. Lett., 25, 273
Roberts, D. A., Goldstein, M. L., Matthaeus, W. H., & Ghosh, S. 1992, J. Geophys. Res., 97, 17115
Rybansky, M., Rusin, V., Minarovjech, M., & Gaspar, P. 1994, Sol. Phys., 152, 153
Smith, C. W., Stawarz, J. E., Vasquez, B. J., et al. 2009, Phys. Rev. Lett., 103, 201101
Smith, E. J., Balogh, A., Neugebauer, M., & McComas, D. 1995a, Geophys. Res. Lett., 22, 3381
Smith, E. J., Marsden, R. G., & Page, D. E. 1995b, Science, 268, 1005
Sorriso-Valvo, L., Carbone, V., Marino, R., et al. 2010, Phys. Rev. Lett., 104, 189002
Sorriso-Valvo, L., Carbone, V., Noullez, A., et al. 2002, Phys. Plasmas, 9, 89
Sorriso-Valvo, L., Carbone, V., Veltri, P., Consolini, G., & Bruno, R. 1999, Geophys. Res. Lett., 26, 1801
Sorriso-Valvo, L., Marino, R., Carbone, V., et al. 2007, Phys. Rev. Lett., 99, 115001
Stawarz, J., Vasquez, B. J., Smith, C. W., Forman, M. A., & Klewicki, J. 2011, ApJ, 736, 44
Wang, Y.-M., Robbrecht, E., & Sheeley, N. R., Jr. 2009, ApJ, 707, 1372
Zhou, Y., & Matthaeus, W. H. 1990, J. Geophys. Res., 95, 14881

The Astrophysical Journal, 752:77 (1pp), 2012 June 10 doi:10.1088/0004-637X/752/1/77

ERRATUM: "ON THE OCCURRENCE OF THE THIRD-ORDER SCALING IN HIGH-LATITUDE SOLAR WIND" (2012, ApJ, 750, 41)

R. Marino[1,2], L. Sorriso-Valvo[3], R. D'Amicis[1], V. Carbone[3,4], R. Bruno[1], and P. Veltri[4]
[1] IFSI-INAF, via Fosso del Cavaliere, 00133 Roma, Italy; raffaele.marino@fis.unical.it
[2] Computational and Information Systems Laboratory, NCAR, P.O. Box 3000, Boulder, CO 80307-3000, USA
[3] IPCF-CNR, U.O. Cosenza, Ponte P. Bucci, cubo 31C, 87036 Rende (CS), Italy
[4] Dipartimento di Fisica, Università della Calabria, Ponte P. Bucci, cubo 31C, 87036 Rende (CS), Italy
Received 2012 May 2; published 2012 May 25

Due to an error at the publisher the inset text was deleted from Figure 4 of the published paper, thereby obscuring its meaning. The corrected figure appears below. IOP Publishing sincerely regrets this error.

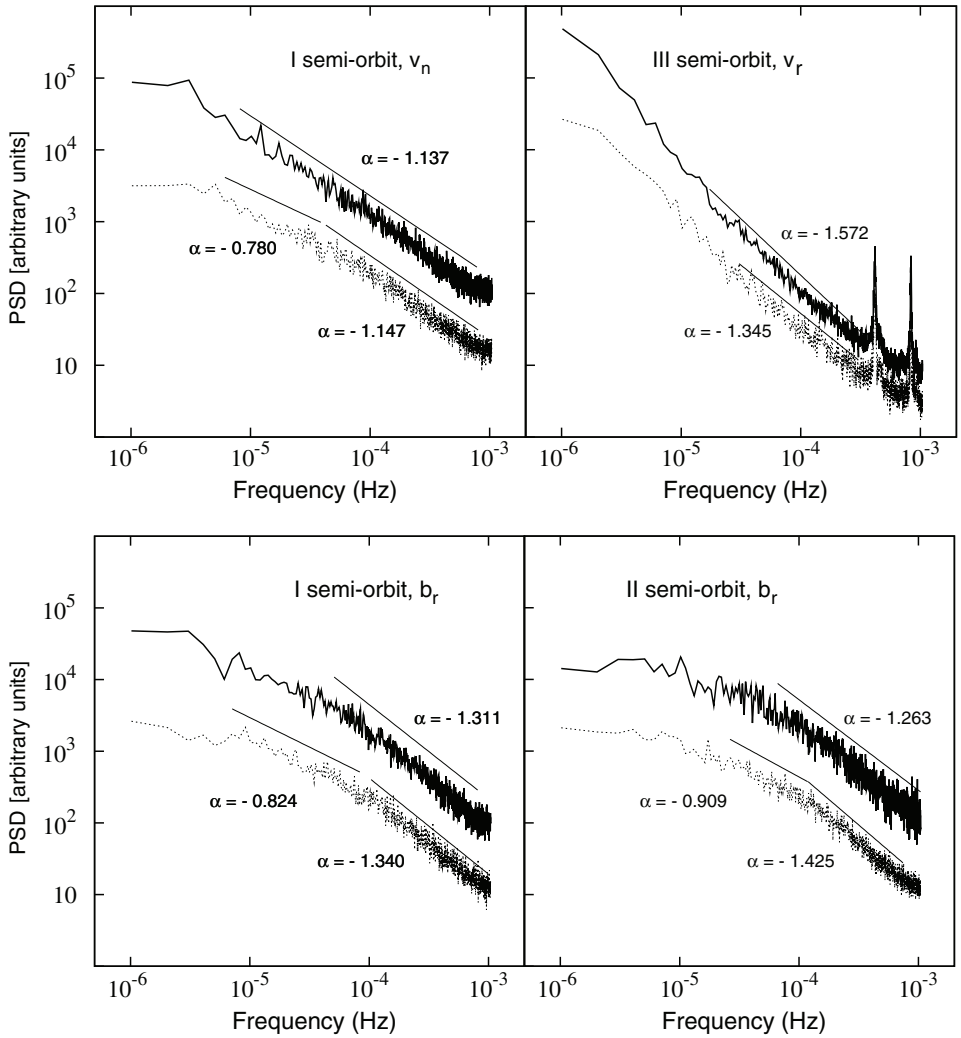

Figure 4. Examples of velocity (top panels) and magnetic field (bottom panels) components power spectra. The spectra are computed separately for regions with (full line) and without (dashed line) Yaglom scaling. Spectra have been vertically shifted for clarity and are given in arbitrary units. Solid lines are power-law fits of the spectra, also vertically shifted for clarity. The spectral indices obtained by the fit are given in the following. Top left panel, solid line: $\alpha = -1.137 \pm 0.001$; dashed lines: -0.780 ± 0.004 and -1.147 ± 0.002. Top right panel, solid line: $\alpha = -1.572 \pm 0.006$; dashed lines: $\alpha = -1.345 \pm 0.006$. Bottom right panel, solid line: $\alpha = -1.263 \pm 0.002$; dashed lines: $\alpha = -0.909 \pm 0.004$ and $\alpha = -1.425 \pm 0.003$. Bottom left panel, solid line: $\alpha = -1.311 \pm 0.002$; dashed lines: $\alpha = -0.824 \pm 0.002$ and $\alpha = -1.340 \pm 0.003$. The two peaks present at high frequency in the v_R spectra are due to the plasma instrument data acquisition logic, see http://ulysses-ops.jpl.esa.int/ulysses/.